NANO LETTERS

2006
Vol. 6, No. 4
755−759

Local Field Effects on Electron Transport in Nanostructured TiO_2 Revealed by Terahertz Spectroscopy

E. Hendry,*,† M. Koeberg,† B. O'Regan,‡ and M. Bonn†

FOM Institute for Atomic and Molecular Physics, Kruislaan 407, 1098 SJ, Amsterdam, The Netherlands, and Chemistry Building, Imperial College, Exhibition Road, London, SW7 2AY, U.K.

Received January 5, 2006; Revised Manuscript Received March 15, 2006

ABSTRACT

We study electron mobilities in nanoporous and single-crystal titanium dioxide with terahertz time domain spectroscopy. This ultrafast technique allows the determination of the electron mobility *after* carrier thermalization with the lattice but *before* equilibration with defect trapping states. The mobilities reported here for single-crystal rutile (1 $cm^2/(V\ s)$) and porous TiO_2 (10^{-2} $cm^2/(V\ s)$) therefore represent upper limits for electron transport at room temperature for defect-free materials. The large difference in mobility between bulk and porous samples is explained using Maxwell–Garnett effective medium theory. These results demonstrate that electron mobility is strongly dependent on the material morphology in nanostructured polar materials due to local field effects and cannot be used as a direct measure of the diffusion coefficient.

In the past decade, dye-sensitized solar (Grätzel) cells[1] have emerged as promising alternatives to traditional silicon solar cells. Grätzel cells consist of a porous network of titanium dioxide (TiO_2) nanoparticles, sensitized with dye molecules, acting as a transport matrix for photoinjected electrons. Transport of charges through the TiO_2 matrix is essential to the functioning of these cells, and good transport characteristics are necessary for a good quantum efficiency of charge collection after injection, particularly in solid-state cells where recombination is faster and competes with charge collection at the outer electrodes.[2] Understanding the transport properties of the porous TiO_2 network is therefore critical for the design of new devices and improving cell efficiency.

Electrons in TiO_2 have an inherently low mobility due to strong electron−phonon interactions that give rise to polaron formation.[3] The highly polarizable TiO_2 lattice deforms around the electron, increasing the electron effective mass and lowering its mobility. Since, at room temperature, both the polaron mean free path and polaron size in TiO_2 (both ∼1 nm in rutile TiO_2 [3,4]) are significantly smaller than the typical ∼25 nm diameter of particles used in Grätzel cells, scattering processes in nanostructures should be dominated by bulk TiO_2 properties. It is therefore remarkable that the macroscopic room-temperature mobility of photogenerated electrons in *porous* TiO_2 ($\sim 7 \times 10^{-6}$ $cm^2/(V\ s)$ determined using time-of-flight measurements[5,6]) is *many orders of magnitude* smaller than that in the bulk material (∼1 $cm^2/(V\ s)$),[3] indicating that electron−phonon momentum relaxation is not the limiting process in the porous sample. Two possible origins for this reduced mobility have previously been proposed:[7] the (temporary) immobilization of electrons at trapping sites and the intrinsic reduction in mobility due to path restrictions imposed by the porous geometry.

In this contribution, we reveal that the origin of this discrepancy in mobility lies not only in these two effects that influence the long-time mobility but also with local field effects that act to reduce the electric field in TiO_2 matrix, even on very short (picosecond) time scales, where trapping has not yet occurred and mobility is largely limited by intraparticle transport.

The rutile single crystal sample, grown commercially by Crystal GmbH, is 1 mm thick (001) cut, and we study the conductivity with the terahertz (THz) electric field perpendicular to the **c** axis. The nanoporous sample is several micrometers thick Degussa P25 TiO_2 (particles of 25 nm diameter), consisting of a mixture of anatase and rutile type TiO_2, spun onto a 1 mm thick quartz substrate. The band gap of rutile at room temperature is 2.9 eV, and slightly higher for anatase.[8] The samples are photoexcited using 150 fs laser pulses with a central wavelength of either 266 or 400 nm (fluence ∼4 J m^{-2}). The samples are mounted in a closed-cycle helium cryostat to allow temperature control in the range 10−300 K.

The conductivity is investigated with THz time domain spectroscopy using an experimental setup similar to that

* To whom correspondence may be addressed. Fax: +31-20-6684106. E-mail: hendry@amolf.nl.
† FOM Institute for Atomic and Molecular Physics.
‡ Chemistry Building, Imperial College.

10.1021/nl0600225 CCC: $33.50
Published on Web 03/29/2006

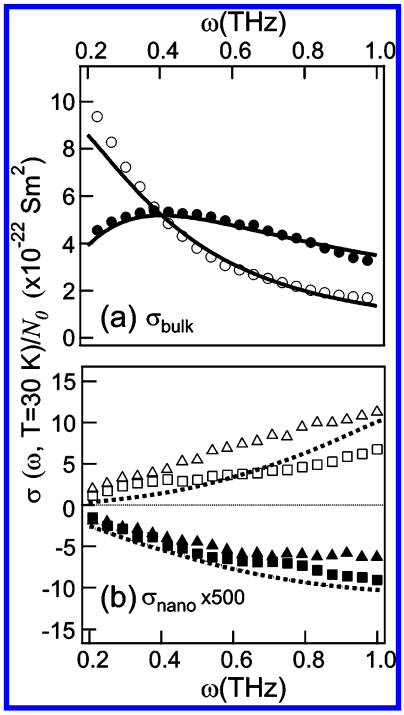

Figure 1. (a) THz conductivity of the single-crystal TiO_2 sample, the real (open symbols) and imaginary (closed symbols) parts, normalized by the excitation density at the sample interface, following excitation by 1.06×10^{18} photons/m^2 (wavelength 266 nm). The full lines are fits to the Drude model. (b) THz conductivity of the porous TiO_2 excited by the same 266 nm fluence (squares). The dotted line is a fit from MG theory scaled by a factor of 3. The triangles show the THz conductivity of dye-sensitized sample excited by 400 nm photons of the same fluence, scaled by a factor of 0.25.

described in detail in ref 9. The THz pulses are essentially single cycle electromagnetic pulses of ~1 ps duration, and the field strength is detected directly in the time domain. The transmissions of these pulses through the unexcited sample $E(t)$, as well as the modulation of this transmission after photoexcitation $\Delta E(t)$, are recorded. Combined with knowledge of the penetration depth l_0 of the excitation light (which determines the spatial charge distribution), the Fourier transforms of the time-domain waveforms yield the complex conductivity $\sigma(\omega)$ at the sample interface in the frequency range 0.1−1.5 THz. When the penetration depth is small compared to the wavelength of the probe light, the sample can be approximated as a thin slab of excited material of thickness l_0 embedded in homogeneous material with a dielectric function ϵ, and the photoconductivity is given by[10]

$$\sigma(\omega) = -\frac{2\epsilon_0 c\sqrt{\epsilon}}{l_0}\frac{\Delta E(\omega)}{E(\omega)} \qquad (1)$$

where ϵ_0 is the permittivity of a vacuum and c is the speed of light. Note that, as $\sigma(\omega)$ is proportional to the charge density, $\sigma(\omega)$ varies with the penetration depth l_0; we therefore report the conductivity normalized by the estimated charge density at the interface N_0.[11]

In Figure 1, the conductivity of single-crystal rutile is compared to that of the porous TiO_2 sample. The conductivities (dominated by the electron response[3]) are measured 10 ps after excitation, i.e. after thermalization of the charge distribution but before any decrease is observed due to carrier trapping, which occurs on longer time scales. The measurements have been carried out using the same excitation fluence (266 nm, 1.06×10^{18} photons/m^2, low enough to avoid charge−charge interaction effects[12]) and measured at $T =$ 30 K, below the onset of significant scattering from optical phonons.[3] From the excitation fluence and penetration depth, N_0 is calculated[11] to be $\sim 2.6 \times 10^{25}$ m^{-3} and $\sim 7.6 \times 10^{24}$ for single crystal and nanoporous samples, respectively.

The most striking feature of the data in Figure 1 is that the normalized THz conductivity in nanoporous TiO_2 is more than 2 orders of magnitude lower than that in the bulk rutile. The conductivity in bulk rutile is described fairly well by the Drude model (full lines in the upper panel in Figure 1)

$$\sigma(\omega) = \epsilon_0 \omega_p^2 \tau_r/(1 - i\omega\tau_r) \qquad (2)$$

with plasma frequency $\omega_p = 260$ THz and momentum relaxation time $\tau_r = 0.4$ ps. The frequency dependence of the conductivity in the nanoporous sample, meanwhile, is very different, and the imaginary component is even opposite in sign (Figure 1b). We observe a similar frequency dependence in a dye-sensitized porous sample[13] excited by 400 nm pulses (~1×10^{18} photons/m^2, see triangles in Figure 1). The conductivity in the dye-sensitized sample is around a factor of 4 larger than that in the bare porous sample. This discrepancy is discussed later.

The distinctive THz response of porous TiO_2 observed in Figure 1b is very similar to that previously observed by Turner et al.[13] for dye-sensitized samples with similar estimated electron densities. In this reference, the authors attributed this unusual frequency dependence to backscattering of electrons due to the finite size of the particles. However, the mean free paths of electrons in rutile have been shown to be appreciably smaller (~1 nm)[3] than the particle size (~25 nm), implying that surface scattering is negligibly small. The effective conductivity measured in the *inhomogeneous* TiO_2 sample must, however, be treated within effective medium theory as described below.

The porous rutile sample is a sintered composite of TiO_2 nanoparticles, i.e., it is an inhomogeneous mix of vacuum and semiconductor regions. We use Maxwell−Garnett (MG) effective medium theory,[14−17] which is valid for spherical particles of diameter smaller than the probe wavelength (~25 nm and ~300 μm, respectively). The effective dielectric function ϵ of the material is then given by that of noninteracting particles, ϵ_p, embedded within a medium ϵ_m (=1 for air)

$$\frac{\epsilon - \epsilon_m}{\epsilon + 2\epsilon_m} = s\frac{\epsilon_p - \epsilon_m}{\epsilon_p + 2\epsilon_m} \qquad (3)$$

where s is the space filling factor. Strictly speaking, eq 3 is correct only to first-order expansion in s[15] and therefore gives exact results in the limit $s \to 0$. Despite this limitation, there

is convincing evidence[17] suggesting that MG theory is applicable to porous, polar materials and indeed has been shown to produce meaningful results[15,16] even for materials with $s \sim 0.5$. For the dielectric function ϵ_p, we use our measured values (at 30 K) for the dielectric function of rutile[4] type TiO_2. The isotropic dielectric function (i.e., for randomly oriented particles) at THz frequencies is then given by $\epsilon_p = (\epsilon_\perp + 2\epsilon_{||})/3 \sim 140$ at 30 K (where $\epsilon_\perp$ and $\epsilon_{||}$ are the dielectric functions perpendicular and parallel to the **c** axis, respectively[4]). The porous TiO_2 used in the experiment has a space filling factor $s \sim 0.5$, such that the effective sample dielectric function at THz frequencies is estimated using eq 3 to be $\epsilon \sim 3.9$, which is consistent with experimentally observed reflective losses from the sample interfaces.

Using MG theory, the effective sample conductivity σ can be related to the local particle conductivity σ_p by setting the sample and local particle dielectric functions in eq 3 to $\epsilon + i\sigma/\omega\epsilon$ and $\epsilon_p + i\sigma_p/\omega\epsilon_0$ respectively, yielding

$$\frac{\epsilon + (i\sigma/\omega\epsilon_0) - \epsilon_m}{\epsilon + (i\sigma/\omega\epsilon_0) + 2\epsilon_m} = s\frac{\epsilon_p + (i\sigma_p/\omega\epsilon_0) - \epsilon_m}{\epsilon_p + (i\sigma_p/\omega\epsilon_0) + 2\epsilon_m} \qquad (4)$$

Combining eqs 3 and 4 and solving for σ yields

$$\sigma = \frac{9s\epsilon_m^2}{s(\epsilon_m - \epsilon_p) + 2\epsilon_m + \epsilon_p} \frac{\sigma_p}{(s(\epsilon_m - \epsilon_p) + 2\epsilon_m + \epsilon_p) - (i\sigma_p(s-1)/\omega\epsilon_0)} \qquad (5)$$

The effective conductivity calculated using eq 5, assuming a Drude model conductivity for σ_p with plasma frequency $\omega_p = 110$ THz and relaxation time $\tau_r = 0.1$ ps, is plotted in Figure 1b (dotted lines). While the frequency dependence and relative amplitude of real and imaginary parts are determined entirely by ω_p and τ_r, the real and imaginary conductivities obtained using eq 5 must be scaled by a factor of 3 in order to reproduce the magnitude of our measured conductivity. The required scaling is expected: it is well-known that MG theory underestimates the magnitude of conductivity for finite values of s.[18] The best fit to the experimental data occurs with a plasma frequency larger (when scaled to N_0), and relaxation time smaller, than those observed for single-crystal rutile in Figure 1a ($\omega_p = 260$ THz and $\tau_r = 0.4$ ps). There are several reasons why this may be: First of all, the purity of the crystal in the nanoporous TiO_2 is not as high as that in the single-crystal sample, so that impurity scattering[19] will play a significant role at these low temperatures. Second, the effective conductivity has been extracted ignoring the mixed phase composition (rutile vs anatase in the approximate ratio 1:3) of the nanoporous TiO_2. From measurements of epitaxial and polycrystalline thin films, there is some suggestion that the intrinsic dielectric function of anatase is significantly lower (in the range of 50−80[20,21]) than that of rutile. Assuming a lower particle dielectric function in eq 5 would allow for better fits to our data with smaller values of ω_p. In any case, it is clear that effective medium theory reproduces the main features of the measured data (conductivity over 2 orders of magnitude smaller than that in bulk, an increasing conductivity with frequency, and a negative imaginary component). The deviation from the more common Drude response for the porous TiO_2 sample results from a resonance in the conductivity: from the denominator in eq 5 it is evident that MG theory introduces a resonance at a frequency where the particle conductivity term $(i\sigma_p(s-1)/\omega\epsilon_0)$ is comparable in size to the lattice dielectric term $(s(\epsilon_m - \epsilon_p) + 2\epsilon_m + \epsilon_p))$. A similar frequency dependence was noted in the conductivity of silicon particles.[10] Though similar THz conductivities have been measured on other porous samples (see for example refs 10 and 13), to our knowledge we are the first to interpret the THz conductivity using effective medium theory.[22]

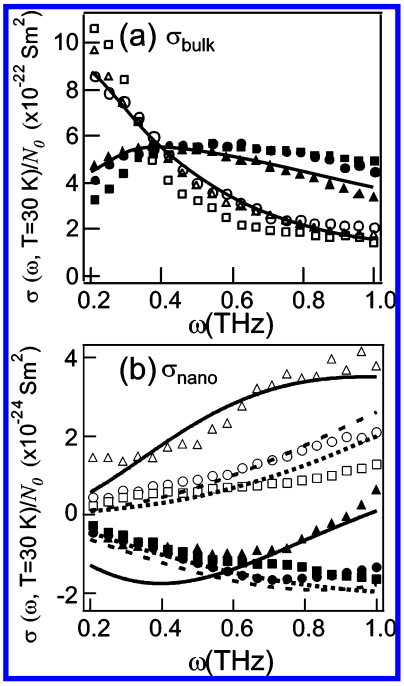

Figure 2. (a) Conductivity (open and filled symbols for real and imaginary parts, respectively) measured at 30 K in single-crystal TiO_2 for excitation fluences of 0.40×10^{18} photons/m^2 (triangles), 0.82×10^{18} photons/m^2 (circles), and 1.06×10^{18} photons/m^2 (squares). The lines represent a fit with the Drude model. (b) Effective conductivity in nanoporous TiO_2 for the same excitation fluences. The lines represent fits from MG theory.

The excitation fluence dependence of the normalized conductivity in nanoporous TiO_2 is also very different from that of bulk rutile. While, at these excitation densities, the normalized conductivity in bulk rutile is essentially independent of excitation fluence (see Figure 2a), the normalized conductivity in nanoporous TiO_2 is strongly density dependent (see Figure 2b, plotted for excitation fluences 0.40×10^{18}, 0.82×10^{18}, and 1.06×10^{18} photons/m^2, corresponding to excitation densities $N_0 \sim 2.8 \times 10^{24}$, 5.8×10^{24}, and 7.6×10^{24} m^{-3}, respectively). Scaling the plasma frequency in the expression for σ_p accordingly, we can reproduce the features in the measured data fairly well (see lines in the lower panel of Figure 2). The variation of the frequency-dependent conductivity with carrier density can fully be accounted for by MG effective medium theory, with the very

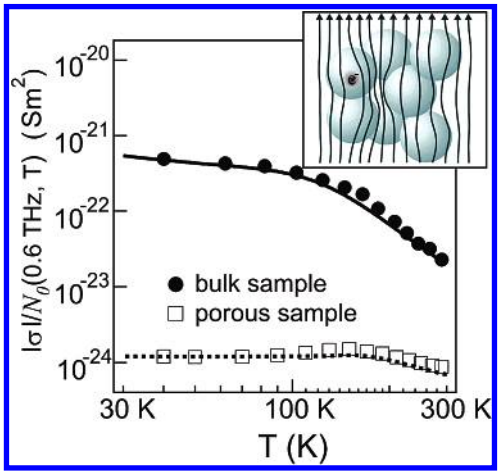

Figure 3. Temperature dependence of the conductivity at 0.6 THz in single-crystal rutile (filled circles) and nanoporous TiO_2 (open squares). The solid line is the temperature dependence predicted by the Drude model, with the relaxation time dominated by electron-optical phonon scattering,[3] given the temperature-dependent THz dielectric function in bulk rutile.[4] The dotted line represents the much weaker temperature dependent conductivity expected for these effects within MG theory with the same temperature-dependent parameters. Inset: Schematic representation of the field lines (arrows) in a porous material: distortion due to shielding by the highly polarizable component particles leads to a redistribution of field strength from the particle (dark gray) to the medium (light gray). The local field experienced by an electron inside a particle is lowered from that experienced by an electron in the bulk material, leading to significantly lower conductivities in porous materials.

strong nonlinearity of response with fluence occurring when $(i\sigma_p(s-1)/\omega\epsilon_0)$ is comparable in size to $(s(\epsilon_m-\epsilon_p)+2\epsilon_m+\epsilon_p))$ in our THz frequency range.

MG theory also predicts the much weaker temperature dependence observed in nanoporous TiO_2 compared to bulk rutile (see Figure 3). The fit (dotted line) has been calculated using eq 5, assuming the temperature dependence of the THz dielectric function[4] and electron−phonon scattering time[3] observed in bulk rutile. Both these quantities have been averaged over the two crystal directions. MG theory also reproduces the maximum in conductivity observed in the region 100−150 K, resulting from the temperature dependence of the static dielectric function ϵ_p[4] and the Drude relaxation time τ_r.[3,4]

For the low densities of mobile electrons ($<10^{22}$ m^{-3}) and high temperatures (∼300 K) applicable to operational solar cells, the small particle conductivity means that eq 5 may be approximated by

$$\sigma = \frac{9s\epsilon_m^{\,2}}{(s(\epsilon_m-\epsilon_p)+2\epsilon_m+\epsilon_p)^2}\,\sigma_p \qquad (6)$$

Using the directionally averaged THz dielectric function of bulk rutile[4] ($\epsilon_p = (\epsilon_\perp + 2\epsilon_{||})/3 \sim 100$ at 300 K), MG theory predicts that the conductivity in porous TiO_2 with $s \sim 0.5$ is reduced from that in the bulk material by roughly 3 orders of magnitude. Microscopically, this apparent reduction in conductivity arises from induced dipoles in the highly polarizable particles which screen the applied electric field, resulting in a larger flux density in the medium (in this case air) than in the TiO_2 (see inset of Figure 3). The local field experienced by an electron inside one of these particles is then lowered from that expected for a homogeneous sample, resulting in a lower effective conductivity. In practice, the difference is somewhat smaller, as MG theory underestimates the conductivity for finite values of s.[18] Indeed, at 300 K the *measured* conductivity in the porous sample is only ∼2 orders of magnitude smaller than that in the bulk material (see Figure 3).

The *mobility*, the quantity determining the motion of charges in response to an *electric field*, is found by comparing the measured conductivities with calculated excitation densities,[11] to be ∼1 $cm^2/(V\ s)$ and $\sim 10^{-2}$ $cm^2/(V\ s)$ for the bulk and nanoporous material, respectively. These values represent mobilities on very short time scales (∼10 ps, before any decrease in conductivity is observed due to carrier trapping) where mobility is largely limited by *intra*particle transport. On longer time scales, restrictions on the random walk of charges through the porous network,[7] charge trapping,[7,23] and possible barriers for *inter*particle transport explain the even lower steady-state mobilities ($\sim 7\times10^{-6}$ $cm^2/(V\ s)$[5,6]) for porous TiO_2. Our results indicate that, while a reduction from the bulk mobility of at least 3 orders of magnitude *is* expected due to these long time effects, an *additional* 2 order of magnitude decrease in mobility is expected from screening of the electric field.

In a conventional solar cell based on a p−n semiconductor junction, the electric field which drives the current arises from the charge density gradient within the cell. In solid-state TiO_2 cells, in which the pores are filled by a hole transporting material, the local field effects described here will be slightly modified,[24] as the contrast between ϵ_m and ϵ_p (the dielectric functions of the hole transporter material and the TiO_2 matrix, respectively) is lower. In these cells, an increase in electron mobility (and corresponding lowering of the cell internal resistance and higher efficiency) may be possible if ϵ_m and ϵ_p can be optimized. Indeed, such a reduction in the contrast between ϵ_m and ϵ_p may explain the larger THz conductivity for a dye-sensitized porous sample compared to the unsensitized sample (plotted in Figure 1b).

In the more common liquid electrolyte Grätzel cell,[1] screening by the ionic *electrolyte* further lowers the local electric fields.[25,26] Indeed, screening by the electrolyte may even be so strong that *diffusion* to the outer electrodes could be the predominant charge transport mechanism.[27] Though the carrier *mobility* is strongly affected by screening of the electric field, this is not expected to influence *diffusion*. From our measurements on the bulk sample, we estimate (using the Einstein relation) that rutile has a diffusion coefficient $D \approx 0.025$ cm^2/s at room temperature. As with mobility, the diffusion coefficient in the porous sample will also be changing with time, depending on defect-related effects such as trapping. For the 3 orders of magnitude decrease we observe in mobility between the short time (THz) and steady state (time-of-flight[5]) mobilities, we estimate a steady-state, room-temperature diffusion constant $\approx 10^{-5}-10^{-4}$ cm^2/s for

the porous sample. This estimate is very comparable to other direct measurements of the steady-state diffusion constants ($\sim 1 \times 10^{-4}$ cm^2/s[7] and $\sim 2 \times 10^{-5}$ cm^2/s[28]) for similar excitation densities in porous TiO_2. It is, however, noticeably larger than diffusion constants inferred (using the Einstein relation) from direct measurements of mobility ($\sim 2 \times 10^{-7}$ cm^2/s determined from flight measurements[5,6]) demonstrating that the determination of charge diffusion coefficients in porous materials should be performed with extreme care when using experimental methods which rely on an applied electric field due to the inhomogeneous distribution of electric field in the sample.

To conclude, we have compared the photoconductivity of single crystal and porous TiO_2 using THz time domain spectroscopy. This technique is unique in that it measures the *short-time* mobility, the average mobility of charges on a $\sim$10 ps time scale. As such, this approach is not sensitive to time spent in defect states and traps, or barriers for charge motion between particles in the porous material. The THz mobilities for bulk[3] (~ 1 cm^2/(V s)) and porous ($\sim 10^{-2}$ cm^2/(V s)) TiO_2 therefore represent intrinsic, upper limits for electron mobilities in these materials. The reduced THz mobility observed in the porous sample results from screening of the applied field by the polar TiO_2 matrix, and is fully accounted for using Maxwell−Garnet effective medium theory. The results presented here show that screening of the applied field results in a significant reduction in charge mobility for polar, porous materials, besides the well-known restrictions on the mobility due to the random walk of charges through the porous network[7] and charge trapping at defects,[7,23] that both result in a further reduction of mobility over long time scales to $<10^{-5}$ cm^2/(V s)[5] for porous TiO_2.

Acknowledgment. This work is part of the research program of the "Stichting voor Fundamenteel Onderzoek der Materie (FOM)", which is financially supported by the "Nederlandse organisatie voor Wetenschappelijk Onderzoek (NWO)".

References

(1) Oregan, B.; Gratzel, M. *Nature* **1991**, *353*, 737.
(2) Kroon, J. M.; O'Regan, B. C.; Roosmalen, J. A. M. v.; Sinke, W. C., Dye- Sensitized Solar Cells. In *Handbook of Photochemistry and Photobiology*; Nalwa, H. S., Ed.; American Scientific Publishers: Stevenson Ranch, CA, 2003; Vol. 1.
(3) Hendry, E.; Wang, F.; Shan, J.; Heinz, T. F.; Bonn, M. *Phys. Rev. B* **2004**, *69*, 081101.
(4) Hendry, E.; Bonn, M.; Wang, F.; Shan, J.; Heinz, T. F. Intermediate sized polarons in rutile type TiO_2. In preparation.
(5) Dittrich, T. *Phys. Status Solidi A* **2000**, *182*, 447.
(6) Dittrich, T. *Phys. Status Solidi A* **1998**, *165*, R5.
(7) Kopidakis, N.; Schiff, E. A.; Park, N. G.; Lagemaat, J. v. d.; Frank, A. J. *J. Phys. Chem. B* **2000**, *104*, 3930.
(8) Tang, H.; Levy, F.; Berger, H.; Schmid, P. E. *Phys. Rev. B* **1995**, *52*, 7771.
(9) Beard, M. C.; Turner, G. M.; Schmuttenmaer, C. A. *J. Phys. Chem. B* **2002**, *106*, 7146.
(10) Nienhuys, H. K.; Sundstrom, V. *Appl. Phys. Lett.* **2005**, *87*, 012101.
(11) The excitation density at the sample interface is calculated from $N_0 \approx (f_l/l_0)|(2/(1+\sqrt{\epsilon_{exc}}))^2|$, where f_l is the excitation fluence and ϵ_{exc} is the material dielectric function at 266 nm. The second term in this equation accounts for reflection losses at the sample interface. For the excitation pulse used in the experiment (266 nm, 4.65 eV), the dielectric function of bulk rutile is $\epsilon_{exc} \sim 1.8 + 10.2i$ (Cardona, M.; Harbeke, G. *Phys. Rev.* **1965**, 137, 1467), corresponding to a penetration depth $l_0 \sim 10$ nm. The effective dielectric function for the porous sample is calculated from eq 3 to be $\epsilon_{exc} \sim 3.1 + 1.0i$, from which a penetration depth $l_0 \sim 70$ nm is inferred. Note that although uncertainties in the precise carrier density (from uncertainties in excitation density and penetration depth) result in significant error bars in the *absolute* number for $\sigma(\omega)$, since the photomodulation of the THz pulse is essentially proportional to the *product* of density *and* penetration depth, a relative comparison *between* the normalized conductivities of different samples, as here, remains unaffected.
(12) Hendry, E.; Koeberg, M.; Pijpers, J.; Bonn, M. Charge−charge interactions in semiconductors probed with THz spectroscopy. In preparation.
(13) Turner, G. M.; Beard, M. C.; Schmuttenmaer, C. A. *J. Phys. Chem. B* **2002**, *106*, 11716.
(14) Kirchner, A.; Busch, K.; Soukoulis, C. M. *Phys. Rev. B* **1998**, *57*, 277.
(15) Spanier, J. E.; Herman, I. P. *Phys. Rev. B* **2000**, *61*, 10437.
(16) Granqvist, C. G.; Hunderi, O. *Phys. Rev. B* **1978**, *18*, 2897.
(17) Gittleman, J. I.; Abeles, B. *Phys. Rev. B* **1977**, *15*, 3273.
(18) Campo, M. A.; Woo, L. Y.; Manson, T. O.; Garboczi, E. J. *J. Electroceram.* **2002**, *9*, 49.
(19) Shan, J.; Wang, F.; Knoesel, E.; Bonn, M.; Heinz, T. F. *Phys. Rev. Lett.* **2003**, *90*, 247401.
(20) Park, B. H.; Li, L. S.; Gibbons, J.; Huang, J. Y.; Jia, Q. X. *Appl. Phys. Lett.* **2001**, *79*, 2797.
(21) Fukuda, H.; Namioka, S.; Miura, M.; Ishikawa, Y.; Yoshino, M.; Nomura, S. *Jpn. J. Appl. Phys.* **1999**, *38*, 6034.
(22) Indeed, it should be noted that eq 5 gives the resonance condition assumed in ref 10 (at frequency $\omega = \omega_p/\sqrt{3}$) in the limits $\omega \gg 1/\tau_r$, $\epsilon_m = 1$, $\epsilon_p = 1$, and $s \rightarrow 0$. While these approximations are reasonable for dilute *metal* nanoparticle samples which resonate in the visible region of the electromagnetic spectrum (for which, indeed, the resonance condition $\omega = \omega_p/\sqrt{3}$ is derived (Kreibig, U.; Vollmer, M. *Optical Properties of Metal Clusters*; Springer: Berlin, 1995)), they are drastic approximations to make for *semiconductor* nanoparticles, which resonate in the THz frequency range.
(23) Anta, J. A.; Nelson, J.; Quirke, N. *Phys. Rev. B* **2002**, *65*, 125324.
(24) O'Regan, B.; Kroeger, J.; Verhees, W.; Durrant, J. Using Photovoltage Rise time to examine charge transport in OMeTAD and liquid cells. In preparation.
(25) Kytin, V. *Phys. Rev. B* **2003**, *68*, 195308.
(26) Screening of the electric field by an electrolyte solution can also be described within the framework of MG theory by introducing an additional conductivity term σ_m in eq 4. Under normal operating conditions of a Gratzel cell, the ion concentration is at least 2 orders of magnitude larger than the electron density, so that $\sigma_p \ll \sigma_m$.
(27) O'Regan, B.; Moser, J.; Anderson, M.; Gratzel, M. *J. Phys. Chem.* **1990**, *94*, 8720.
(28) Solbrand, A.; Lindstrom, H.; Rensmo, H.; Hagfeldt, A.; Lindquist, S. E.; Sodergren, S. *J. Phys. Chem. B* **1997**, *101* (14), 2514.

NL0600225